Colloid Polym Sci 278:830–840 (2000)

ORIGINAL CONTRIBUTION

H. Senff
W. Richtering

Influence of cross-link density on rheological properties of temperature-sensitive microgel suspensions

Received: 15 December 1999
Accepted: 15 February 2000

H. Senff · W. Richtering (✉)
Institut für Makromolekulare Chemie
Albert-Ludwigs-Universität Freiburg
Stefan-Meier-Strasse 31
79104 Freiburg, Germany
e-mail: rich@uni-freiburg.de
Tel.: +49-761-2036304
Fax: +49-761-2036319

Abstract The influence of the cross-link density on rheological properties of thermosensitive microgels was investigated. The temperature-sensitive hydrogel particles consisted of poly (*N*-isopropylacrylamide) (PNiPAM) chemically cross-linked with several different molar ratios of *N,N′*-methylenebisacrylamide. The variation of cross-link density leads to soft spheres that possess a different particle interaction potential and a different swelling ratio. With increasing temperature the microgel particles decrease in size and with it the effective volume fraction, which leads to strong changes in rheological properties. The relative zero-shear viscosity and the plateau modulus at different temperatures superpose to mastercurves when plotted versus the effective volume fraction. Up to an effective volume fraction of 0.5 the microgels behaved like hard spheres and the maximum volume fraction, as determined from the divergence of the zero-shear viscosity, was mainly dominated by the polydispersity of the spheres and not by the cross-link density. The plateau modulus, on the other hand, revealed soft-sphere behavior and the interaction potential became softer with decreasing cross-linker content.

Key words Temperature-sensitive microgel · Poly(*N*-isopropylacrylamide) · Rheology · Hard spheres · Colloidal suspension

Introduction

Microgels are a class of macromolecules intermediate between highly branched polymers and macroscopic polymer networks [1]. A microgel is an intramolecularly cross-linked, soluble macromolecule of colloidal dimensions. The size depends on the degree of cross-linking and the nature of the solvent and is comparable to very high molecular weight polymers; the internal structure, however, is that of a swollen network [2]. An important application of microgels is the use as binders in organic coatings [3, 4]. Like usual latex particles they reduce the viscosity at high solid contents compared to solutions of linear macromolecules, but in contrast to latices, microgel particles have the advantage of being soluble in the solvent, so no additional stabilization is necessary.

Microgels were first synthesized and described by Staudinger and Husemann [5] in 1935. In 1958 Shashou and Beaman [6] examined the viscosity of microgel particles systematically and they found a reverse proportionality of the viscosity to the molar ratio of cross-linker to monomer from the synthesis. This reflects the decrease in size of a swollen microgel with increasing network density. Furthermore the particle interaction potential strongly depends on the cross-linking density and thus microgels exhibit a behavior ranging from that of polymer solutions to that of hard spheres [7–10]. At intermediate degrees of cross-linking and swelling the microgels start to resemble the behavior of multiarm star polymers or block copolymer micelles [11–13].

In this work *N*-isopropylacrylamide (NiPAM) is used as a monomer which is cross-linked during polymerization with *N,N′*-methylenebisarcylamide (BIS). The resulting PNiPAM microgels show similar thermal behaviour as linear PNiPAM chains in aqueous solution: a demixing upon heating with a lower critical

solution temperature (LCST) of about 33 °C [14–21]. Macroscopic gels display a strong change in volume and can be used for different applications [22].

Due to their temperature sensitivity PNiPAM-based systems are sometimes called ''smart materials'' and several studies have dealt with the influence of comonomers or solvent mixtures on material properties and their use, for example, for drug delivery [23–27].

Using a thermosensitive microgel as a colloidal particle has the advantage of influencing the particle diameter through temperature changes and with it the rheological properties which are generally a function of the volume fraction. In contrast to other colloidal systems, the temperature is an additional parameter to control its attributes; however, there are only few studies on rheological properties of concentrated PNiPAM microgels showing that the temperature-dependent swelling of the particles strongly alters the flow behavior.

In two previous investigations we established that below 30 °C the rheological properties of a thermosensitive core–shell latex [28] and of a thermosensitive microgel [29] fall on a mastercurve. The viscosity and the moduli of these colloidal suspensions are only influenced by the effective particle volume fraction. This indicates that the particle interaction potential does not change significantly at temperatures below 30 °C.

In this contribution, we report investigations of the influence of the cross-link density of thermosensitive PNiPAM microgels on the rheological behavior. Microgels with different amounts of cross-linker were prepared and they were colloidally stable below the LCST of PNiPAM. At high temperatures the microgel particles flocculated; thus, there was no additional electrostatic stabilization present, in contrast to samples investigated in other studies. Flow properties were determined in a broad concentration and temperature range with the intention to investigate whether the cross-link density influences the rheological behavior. We especially focus on the zero-shear viscosity and the plateau modulus.

Experimental

Materials

NiPAM(Aldrich), BIS (Fluka), sodium dodecyl sulfate (SDS; Merck) and potassium peroxodisulfate (KPS; Merck) were used as received. Deionized water (Millipore) was used.

Emulsion polymerization

Emulsion polymerization was done in a 2 l three-necked flask equipped with a stirrer, a reflux condensor and a gas inlet. NiPAM (about 7.9 g, 69.65 mmol), varying amounts of cross-linker BIS (0.065–0.57 g, 0.97 mmol) and stabilizer SDS (about 0.15 g) were dissolved in 450 ml pure water under stirring (see Table 1 for exact compositions). The initiator KPS (about 0.3 g) was dissolved in 50 ml water. Both solutions were bubbled with nitrogen for 30 min. After heating the mixture to 70 °C the initiator solution was added. Polymerization took place for 8 h while the mixture was stirred at 300 rpm. The dispersion was cooled to room temperature and filtered through glass wool. Further purification was done by extensive dialysis against water until the conductivity was less than 1 μS/cm.

The microgels are abbreviated by the molar ratio of monomer to cross-linker (see first and last rows in Table 1). M34 for instance is the microgel with a molar ratio of 34 of NiPAM to BIS in the synthesis. This would result in a theoretical chain length of 17 between two cross-links. Some properties of microgel M71 were discussed previously [29].

Methods

Dynamic light scattering (DLS) experiments were performed with an ALV goniometer and an ALV 5000 correlator at a wavelength of 647 nm. The refractive index increment in water was measured with a Brice–Pheonix differential refractometer. The static light scattering (SLS) experiments were performed with a computer-driven modified SOFICA goniometer at a wavelength of 632.8 nm. The density of the microgels was estimated using a DMA48 apparatus from Anton Paar, Graz, Austria. Differential scanning calorimetry (DSC) measurements were performed with a Perkin-Elmer DSC7 at a rate of 10 K/min. An automatic Schott Micro Ostwald viscosimeter was used to determine the intrinsic viscosity. Rheological properties of concentrated hydrogel dispersions were investigated with a stress-controlled Bohlin CVO rheometer in cone/plate geometry.

Results and discussion

Particle characterization

The thermosensitive PNiPAM particles were characterized in dilute solution by DLS in a temperature range between 7 and 42 °C. The relative change of the hydrodynamic radius, R_h, as a function of temperature is shown in Fig. 1. To compare the different cross-link densities of the microgels, the hydrodynamic radius was normalized by the value at 40 °C. This temperature lies far above the LCST of PNiPAM and for all samples there was no significant change in hydrodynamic radius at temperatures above 38 °C. The absolute values of R_h are listed in Table 2.

Table 1 Compositions for the synthesis of the microgels. *N*-isopropylacrylamide (*NiPAM*), *N*,*N*′-methylene bisacrylamide (*BIS*), Sodium dodecyl sulfate (*SDS*)

Sample	NiPAM (g)	BIS (g)	SDS (g)	$K_2S_2O_8$ (g)	Mass ratio of NiPAM to BIS	Molar ratio of NiPAM to BIS
M165	7.85	0.065	0.15	0.32	120.8	164.6
M71	7.87	0.15	0.15	0.3	52.5	71.5
M34	7.93	0.32	0.15	0.33	24.8	33.8
M19	7.89	0.57	0.16	0.33	13.8	18.9

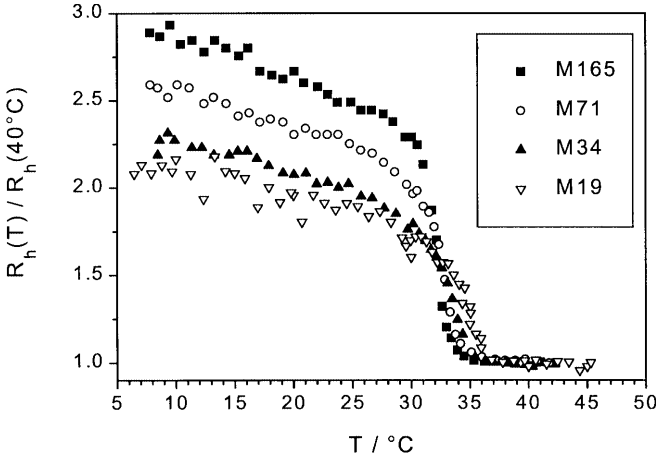

Fig. 1 Normalized hydrodynamic radius of the different poly(*N*-isopropylacrylamide) microgels versus temperature

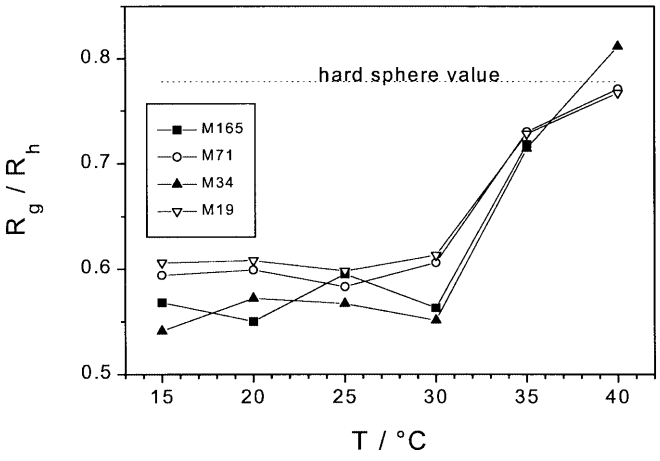

Fig. 2 The ratio $\rho = R_g/R_h$ as a function of the temperature for the microgels M169, M71, M34 and M19. The *dotted line* corresponds to the value of hard spheres with $\rho = 0.778$

Table 2 Hydrodynamic radius of the microgels at different temperatures

Sample	R_h/(nm)						
	10 °C	15 °C	20 °C	25 °C	30 °C	35 °C	40 °C
M165	134	125	122	111	103	47.3	45
M71	142.5	138	131	126	108	57.5	54.5
M34	108	109	100.5	96	88	49	47.5
M19	92	89	87	84	76	53.5	42.6

The temperature-dependent hydrodynamic radius shows a continuous decrease when approaching the LCST. As anticipated, the microgels with a lower cross-linker content are more swellable. The transition temperature is only slightly influenced by the network density. Comparable investigations by Inomata et al. [30] on macroscopic PNiPAM gels have also shown that the temperature of the volume phase transition is nearly independent of the cross-link density; however, the transition near the LCST is influenced by the cross-link density. With increasing cross-linker content the volume phase transition became more continuous, which is caused by the different polarity of BIS.

The microgel solutions were further investigated by SLS. This allows the apparent radius of gyration, $R_{g,app}$, to be determined. The dimensionless ratio $\rho = R_g/R_h$ is called the ρ parameter and has characteristic values for different polymer architectures. For random polymer coils ρ values vary in the range 1.50–1.78 depending on the solvent quality; for hard spheres $\rho = 0.778$ and for microgels ρ is usually smaller than the hard-sphere value [31, 32]. The ρ parameter of the PNiPAM microgels is shown in Fig. 2. It was in the range 0.55–0.6 at temperatures at or below 30 °C and approached the hard-sphere value above 33 °C, when the hydrogel collapsed. These are typical ρ values for microgels. A comparison with data from the literature shows, for instance, that $\rho = 0.5$ for poly(vinyl alcohol) microgels in methanol [31], $\rho = 0.53$ for poly(methyl methacrylate) (PMMA) microgels in tetrahydrofuran [33] and ($\rho = 0.55$–0.65 for PMMA microgels with different cross-link density in butyl carbitol acetate [7]. The low value of around 0.6 is caused by the architecture of the microgel particles. The particles are strongly swollen and the network density decreases at the particle surface, because the cross-linker BIS has a higher polymerization rate compared to the monomer NiPAM [14]; therefore, the core is covered with dangling chains that increase the hydrodynamic radius but have a smaller effect on the radius of gyration and the ρ parameter is expected to be smaller than that of hard spheres. When reaching 33 °C the particles collapse and the ρ parameter approaches the limit of compact spheres.

The microgel particles are highly swollen. The molecular weight of the microgels particles is of the order of 1.5×10^8 g/mol as determined by SLS. Using this molar mass together with the hydrodynamic radius one can compare the effective density inside the microgel particle with the polymer density. This rough estimation suggests that only 5% of the effective volume is occupied by polymer segments for M19. The same calculation for M34 and M71 leads to water contents of 96 and 98%, respectively. Even in the collapsed state the microgels contain a significant amount of water [34].

The volume phase transition was further investigated by DSC. An endothermic peak was found during the heating run and an exothermic peak was found during the cooling run. This is a first-order transition as is found for macroscopic PNiPAM gels [35, 36]. A slight dependence of the transition temperatures on the cross-link density was found, in particular, for the highly

cross-linked microgel M19. This agrees well with the results from light scattering as shown in Fig. 1. The enthalpy change decreased with increasing content of BIS.

The microgels were colloidally stable only below the LCST of PNiPAM and it was not possible to reliably determine the very small electrophoretic mobility of the particles. Both observations indicate that there was no additional electrostatic stabilization present in the microgels investigated in this study.

Rheological behaviour

Viscosity

It is well known that the viscosity of hard-sphere suspensions depends only on the volume fraction of the particles. This concept can also be used for microgels; however, the effective volume fraction, ϕ_{eff}, has to be considered. A simple method to determine this effective volume fraction of colloidal suspensions is the measurement of the relative viscosity, η_{rel}, in dilute solution, which is related to the effective volume fraction via an expression derived by Batchelor for hard-sphere suspensions [37]

$$\eta_{\text{rel}} = \frac{\eta_0}{\eta_s} = 1 + 2.5\phi_{\text{eff}} + 5.9\phi_{\text{eff}}^2 \quad . \tag{1}$$

η_0 and η_s denote the zero-shear viscosity of the suspension and the solvent, respectively. ϕ_{eff} can be substituted by kc, where c is the mass concentration of the dispersion in weight per weight and k is a shift factor for converting the mass concentration to the effective volume fraction.

The relative viscosity of all the dilute PNiPAM microgels is shown in Fig. 3 as a function of the mass concentration for different temperatures. The lines represent fits according to Eq.(1), with ϕ_{eff} substituted by $\phi_{\text{eff}} = kc$. A strong temperature dependence can be seen, which is caused by the shrinkage of the particles with increasing temperature. With decreasing cross-linker content the particles are able to swell more, so the same solid content leads to a higher relative viscosity at all temperatures. The jump between 30 and 35 °C gets smaller with increasing cross-link density. The k shift factors obtained from the fit are summarized in Table 3.

At higher concentrations the microgel suspensions show shear-rate-dependent flow behavior as is known from concentrated dispersions: shear thinning and a second plateau at high shear rates. The viscosity changes strongly with temperature, as is shown in Fig. 4 for a 3.30 wt% M34 sample. Low-shear and high-shear plateaus, η_0 and η_∞, were determined by fitting the data with an equation given by Cross [38],

$$\frac{\eta - \eta_\infty}{\eta_0 - \eta_\infty} = \frac{1}{1 + (\kappa\dot{\gamma})^m} \quad , \tag{2}$$

which is known to provide a good description of the viscosity of colloidal suspensions. The fits according to Eq. (2) are represented by the solid lines in Fig. 4.

For sterically stabilized particles it has been shown by De Kruif et al. [39] that the shear thinning for different volume fractions is a function of the so-called critical shear stress, σ_c. The critical shear stress corresponds to the intermediate viscosity at $\eta = (\eta_0 - \eta_\infty)/2$. A plot of $(\eta - \eta_\infty)/(\eta_0 - \eta_\infty)$ as function of σ/σ_c should give a mastercurve. Figure 5 shows the result for the viscosity curves of M34 already shown in Fig. 4: a master curve is obtained. Taking into account the extreme variation of the viscosity in the low-shear regime by more than 3 orders of magnitude and in the high-shear regime by about 1 order of magnitude, the noise of the data in the low-shear part of the mastercurve is not excessive. A similar calculation for M71 is shown in Fig. 5b at a concentration of 1.96 wt%.

A comparison with other systems is possible via the relative critical shear stress, $\sigma_{c,\text{rel}}$, given by

$$\sigma_{c,\text{rel}} = \frac{a^3\sigma_c}{kT} \quad , \tag{3}$$

with the particle radius a. One example is shown in Fig. 6. The maximum of the relative characteristic shear stress, however, was at a different volume fraction compared to hard-sphere systems, where the maximum was observed at $\phi_{\text{eff}} = 0.5$ [39, 40]. For the PNiPAM microgels we found the maximum at ϕ_{eff} values of about 0.5, 0.4 and 0.3 for M19, M34 and M71, respectively. The maximum shifts to lower ϕ_{eff} with decreasing cross-link density are in agreement with the results of Wolfe and Scopazzi [7].

The viscosity of hard-sphere suspensions at high concentrations is often described with the semi-empirical equations of Krieger and Dougherty [41]

$$\eta = \eta_s\left(1 - \frac{\phi}{\phi_{\max}}\right)^{-[\eta]\phi_{\max}} \tag{4}$$

or Quemada [42]

$$\eta = \eta_s\left(1 - \frac{\phi}{\phi_{\max}}\right)^{-2} \quad . \tag{5}$$

Recently, a mastercurve for the zero-shear viscosity of monodisperse hard-sphere suspensions at high volume fraction was reported by Phan et al. [43] and Meeker et al. [44].

The relative zero-shear and high-shear viscosities of all the microgel samples are plotted versus the *effective* volume fraction in Fig. 7. All the curves at different temperatures follow a single mastercurve. This shows

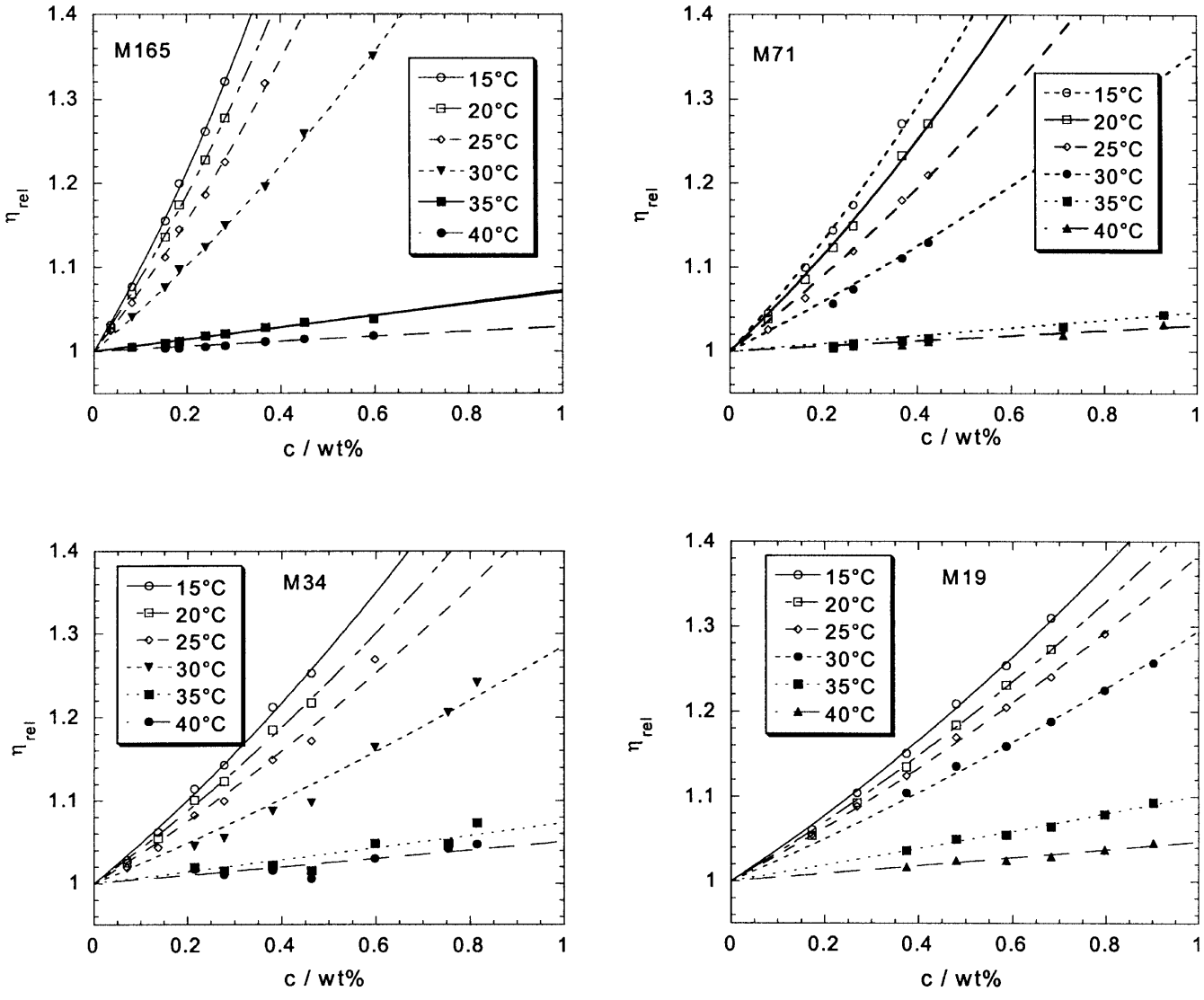

Fig. 3 Relative viscosities of microgels M165, M71, M34 and M19 versus the concentration for six different temperatures with fits according to Eq. (1)

that the shear viscosity is only a function of the *effective* volume fraction of the microgel particles even at high concentration. Obviously, the particle interaction potential does not change significantly in the temperature range investigated.

In Fig. 7 we also plotted a line representing the relative zero-shear viscosity of model hard-sphere suspensions as provided by Meeker et al. [44] Obviously, the microgels resembled hard-sphere behavior up to an effective volume fraction of about 0.5 despite their different degree of cross-linking. This indicates that the solvent within the microgel particles is immobilized at the cross-link densities investigated. In other words, the nondraining limit was reached and the hydrodynamic

Table 3 Shift factors, k, obtained from fitting the viscosity in dilute solution according to Eq. (1)

Sample	$k \times 100$					
	15 °C	20 °C	25 °C	30 °C	35 °C	40 °C
M165	36.55 ± 0.41	32.39 ± 0.37	27.55 ± 0.37	18.77 ± 0.21	2.74 ± 0.08	1.16 ± 0.07
M71	23.75 ± 0.48	20.93 ± 0.33	16.74 ± 0.30	11.31 ± 0.23	1.79 ± 0.06	1.19 ± 0.04
M35	18.49 ± 0.23	16.29 ± 0.23	14.07 ± 0.34	9.36 ± 0.23	2.77	1.95
M19	14.58 ± 0.11	13.19 ± 0.10	11.98 ± 0.07	9.60 ± 0.09	3.73	1.80

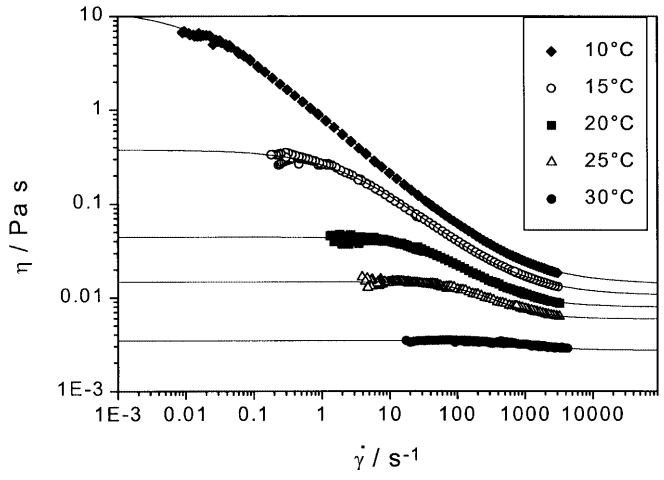

Fig. 4 Shear-rate dependence of the viscosity of microgel M34 with 3.30 wt% for different temperatures. The *solid lines* are fits according to Eq. (2)

properties of the particles are very similar to that of hard spheres. Above an effective volume fraction of 0.5 deviations from hard-sphere behavior can be seen. The zero-shear viscosity diverges at higher effective volume fractions compared to hard spheres.

An exception is the microgel M19, the zero-shear viscosity of which did not diverge. Despite the high cross-link density these particles do not behave like spheres. Obviously, the polymer architecture of M19 is different from that of the other microgels. It resembles the behavior of star polymers with a low arm density. Roovers [11] demonstrated that the viscosity of star polymer solutions approaches hard-sphere behavior with increasing number of arms. Apparently, the M19 microgel particles begin to penetrate each other at the surface and to change the rheological behavior above the overlap concentration, c^*. A simple estimation of the overlap concentration via the intrinsic viscosity is given by $c^* \approx 1/[\eta]$. The value for all temperatures is around $c^* = 0.4$. That is exactly the value where the viscosity deviates from the steep increase as shown in Fig. 7. The different behavior of sample M19 with the highest cross-linker content can be due to different copolymerization parameters of monomer and cross-linker [14]. Since the latter has a higher polymerization rate, an inhomogeneous network is achieved with a concentration profile of the cross-linker from the center to the periphery [45]. At the beginning of the polymerization more cross-linker is incorporated into the microgel, so a highly cross-linked sphere with long polymer chains at the surface is produced – a so-called starlike microgel. It is interesting to note that the different internal structure of microgel M19 was not detected by light scattering in dilute solution. The shear viscosity at high concentration seems to be more sensitive to deviations from the classical microgel architecture.

As already mentioned in the Introduction, it has often been reported that the flow behavior of microgels depends on the cross-link density. One expects that the

Fig. 5 Mastercurves of the shear thinning of M34 (*left*) at 3.3 wt% and M71 (*right*) at 1.96 wt%

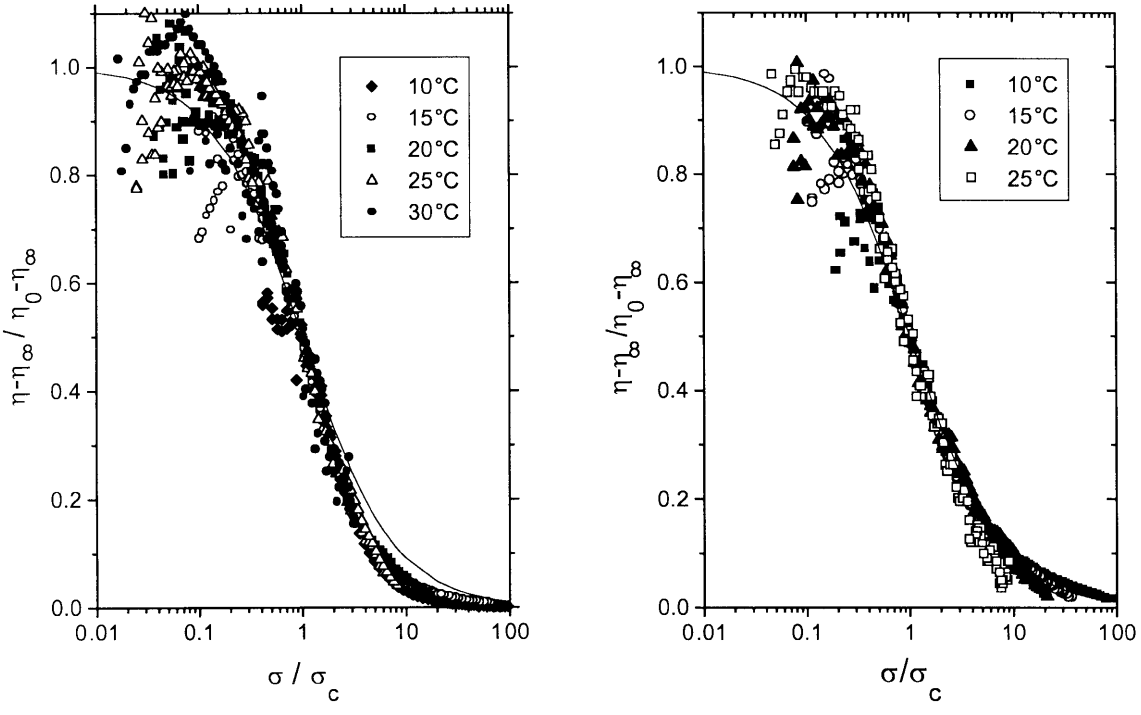

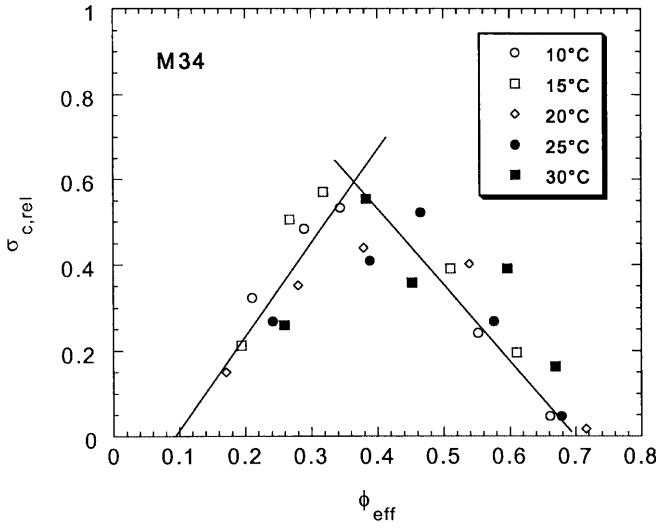

Fig. 6 Relative critical shear stress of M34 as function of the effective volume fraction. The *lines* are to guide the eye

microgels become more hard-sphere-like when the cross-link density increases. Indeed Wolfe and coworkers observed that the relative viscosity approached hard-sphere behavior with increasing degree of cross-linking. The curves in Fig. 7, however, display a slightly different behavior. ϕ_{max}, the effective volume fraction at the divergence of the zero-shear viscosity, does not decrease systematically with decreasing cross-link density. Instead, sample M71, with an intermediate degree of cross-linking, shows the behavior closest to the hard-sphere curve. This points to the important influence of a second parameter, namely the size polydispersity.

It is well known that the size polydispersity strongly influences the colloidal phase behavior of hard spheres [46]. Only samples with low polydispersity can form colloidal crystals and also the glass-transition is affected by the polydispersity. Since the maximum achievable volume fraction depends on the size polydispersity, the divergence of the zero-shear viscosity will not only depend on the interaction potential but also on polydispersity.

The maximum volume fraction for M71 is smaller than that for M34 although M71 has a lower cross-link density and, consequently, a softer interaction potential, so the opposite is expected. The difference between these two microgels is the polydispersity. While M71 has a crystalline phase (Fig. 8), M34 does not form colloidal crystals. Extensive annealing of samples in the concentration range near the maximum volume fraction showed no formation of crystals even after 4 weeks, whereas M71 samples crystallize within 24 h. This means that M71 has a smaller polydispersity because only very monodisperse spheres are able to crystallize. Obviously the polydispersity plays an important role for the maximum packing fraction and seems to be more important for the divergence of the zero-shear viscosity than cross-linking density.

Elastic properties

When the zero-shear viscosity diverges, the microgel particles come into close contact and elastic properties of the densely packed spheres arise. The yield stress and the elastic moduli of concentrated suspensions can be measured. These properties are again a function of the temperature for a microgel dispersion with the same solid content. The yield stress is indicated in Fig. 9: the evolution of shear deformation and shear rate with increasing applied shear stress are shown for M71 at a concentration of 6.86 wt%.

The frequency dependence of the storage and the loss moduli, G' and G'', respectively, was determined in low-amplitude oscillatory-shear experiments. At low temperatures, the sample behaved as a viscoelastic solid: the storage modulus was higher than the loss modulus in the whole frequency range. G' was independent of frequency and corresponds to the plateau modulus, G_p. Upon heating, the sample changed to a viscoelastic liquid with $G'' > G'$ (Fig. 10). G_p decreased with temperature and a mastercurve was obtained when G_p was plotted versus ϕ_{eff} (Fig. 11). The effective volume fractions were again calculated using the shift factors obtained by viscometry in dilute solution. Very high nominal ϕ_{eff} values are again obtained and it is obvious that the microgel particles become compressed at high concentration. However, the influence of temperature on the moduli of the concentrated dispersions cancels out when the swelling behavior of the single particles (as determined by viscometry and DLS) is taken into account.

Often a linear relation is found between G_p and the yield stress, σ_y [47, 48]. For charge-stabilized lattices a ratio of $\sigma_y/G_p = 0.025$ was reported. The yield stress is plotted for all temperatures and concentrations of the microgels versus the plateau modulus in Fig. 12. Again mastercurves are obtained; however, with lower cross-linker content the slope is steeper and the value is much higher than 0.025. The dangling chains on the microgel surface penetrate each other at high volume fractions, which results in a higher yield stress at the given elastic modulus. For M34, M71 and M164 slopes of 0.048, 0.055 and 0.072 are obtained. Obviously, particles with a lower cross-link density have longer chains at the particle surface and these easily penetrate each other at high concentrations and give rise to a higher yield stress. This indicates that the yield stress depends on the chain topology at the surface of the microgel particles, whereas the plateau modulus depends on the cross-link density in the inner part of the microgels.

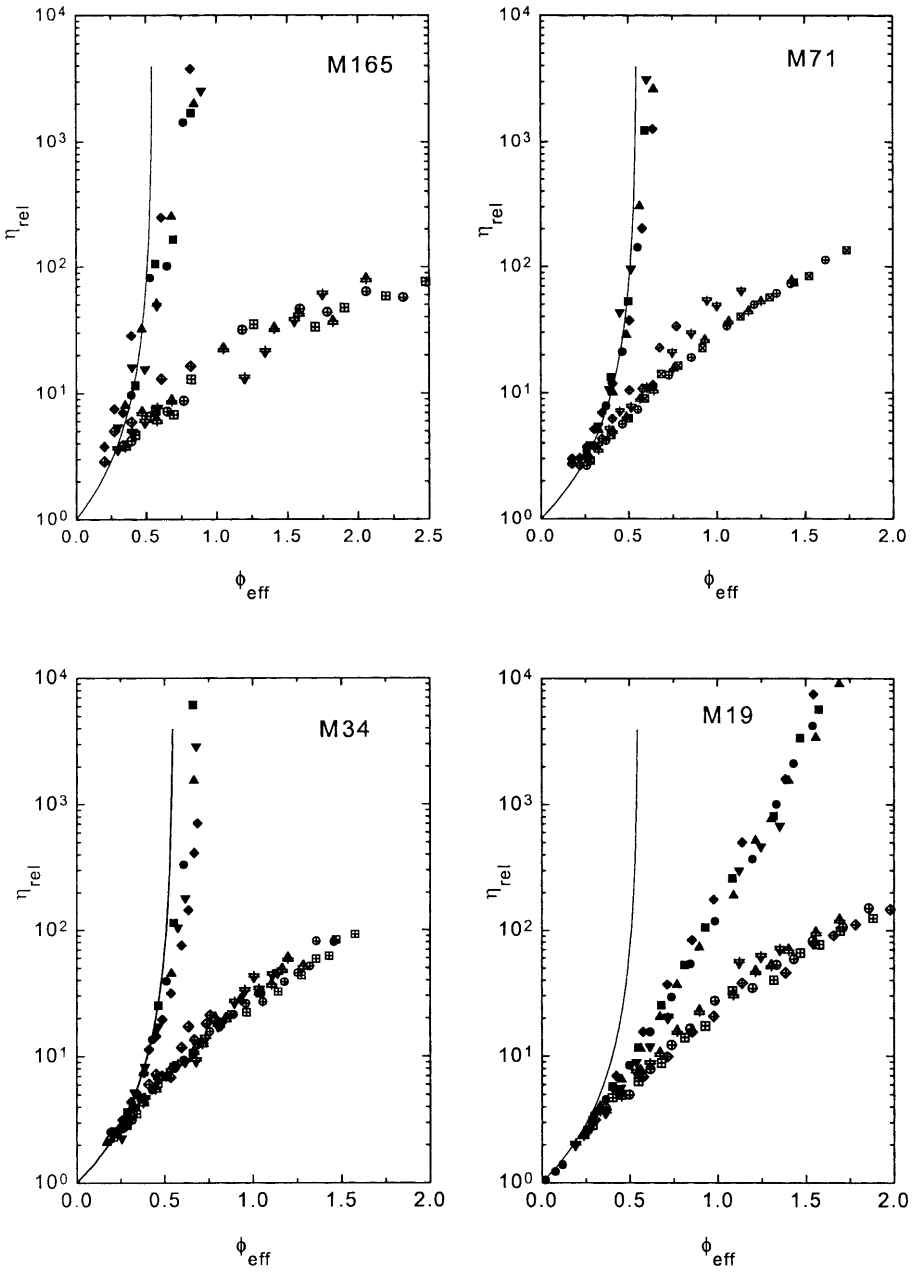

Fig. 7 Relative high-shear (*crossed symbols*) and relative low-shear viscosity (*filled symbols*) of microgels M165, M71, M34 and M19 versus the effective volume fraction for six different temperatures. (■: 10 °C; ●: 15 °C; ▲: 20 °C; ▼: 25 °C; ◆: 30 °C). The *solid line* displays the hard-sphere behavior according to Meeker et al

The elastic plateau modulus can be related to the interaction potential and the pair correlation function by using the Zwanzig and Mountain equation [50–51]:

$$G_{\mathrm{p}} = nkT + \frac{2\pi}{15} n^2 \int_0^{\infty} g(r) \frac{\mathrm{d}}{\mathrm{d}r}\left(r^4 \frac{\mathrm{d}\psi}{\mathrm{d}r}\right) \mathrm{d}r \ . \tag{6}$$

Here n is the particle number density, k Boltzmann's constant, $g(r)$ the radial distribution function, with r the center–center separation, and $\psi(r)$ the pair interaction potential. In concentrated suspensions the particles are arranged at well-defined distances and $g(r)$ can be replaced by a Dirac delta function. By assuming a latticelike microstructure, a rather simple expression can be obtained [52]

$$G_{\mathrm{p}} \propto \frac{1}{r}\left(\frac{\partial^2 \psi}{\partial r^2}\right) \ . \tag{7}$$

Wagner pointed out that Eq. (7) was obtained for simple fluids and the hydrodynamic interaction is neglected. Taking into account hydrodynamic interaction leads to a more complicated expression which also includes the first derivative of $\psi(r)$. Nevertheless, Eq. (7) provides a good fit to experimental data,

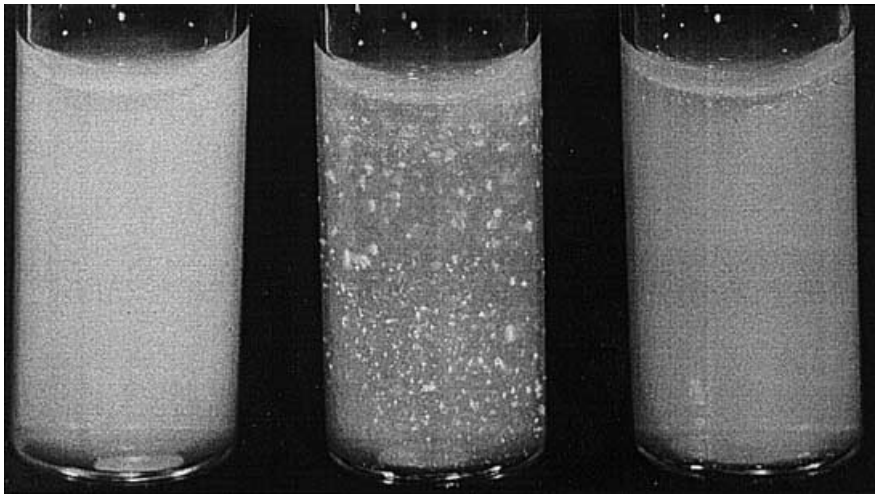

Fig. 8 Colloidal phase behavior of M71 at 15 °C. *Left*: fluid at 2.477 wt%; *middle*: crystalline at 2.765 wt%; *right*: glassy at 3.015 wt%

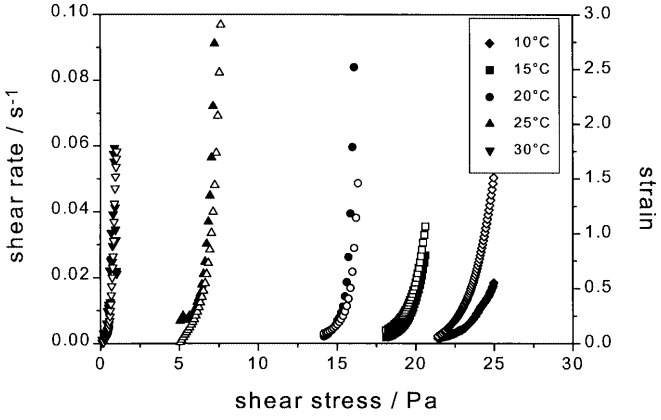

Fig. 9 Yield stress of M71 at 6.86 wt%: shear rate (*filled symbols*) and strain (*open symbols*) as a function of the shear stress for different temperatures

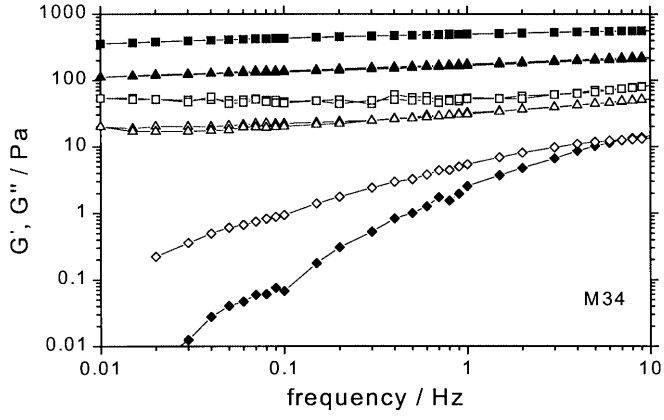

Fig. 10 Elastic modulus, G', (*filled symbols*) and loss modulus, G'', (*open symbols*) versus frequency for M34 at 7.15 wt% and temperatures 10 °C (■), 20 °C (▲) and 30 °C (◆)

probably due to a cancellation of errors when a latticelike structure is assumed and hydrodynamic interactions are neglected.

The interaction potential of concentrated microgel dispersions can be modeled as $\psi(r) \propto 1/r^n$, which gives a power-law behavior for the concentration dependence of the plateau modulus, i.e. $G_p \propto \phi_{eff}^m$. Figure 11 shows a double-logarithmic plot of G_p versus the effective volume fraction for sample M34, and a mastercurve is obtained with the temperature-sensitive PNiPAM microgels. The solid line corresponds to a power-law fit of all data points and has a slope of $m = 5.82$. The slopes for the less cross-linked samples M71 and M164 are 4.9 and 3.19, respectively. These values may be compared to the PMMA microgels investigated by Paulin et al. [53], who found a power-law exponent of $m = 7.7$. The power-law exponent, m, of the plateau modulus is related to the exponent, n, of the interaction potential via $m = 1 + n/3$. Thus, the slope of G_p in Fig. 11 corresponds to $n = 14.5$ and indicates soft-sphere behavior. n for samples M71 and M164 is 11.7 and 6.6, respectively. Thus, the exponent, n, of the interaction potential is correlated with the cross-link density. A higher cross-link density leads to a higher interparticle force as determined by the elastic properties. This is different from the viscosity measurements, where the polydispersity has a strong influence on the volume fraction of the divergence of the zero-shear viscosity.

Now we wish to compare the behavior of the temperature-sensitive microgel particles with other soft-sphere systems, for example, silica particles with long grafted polysiloxane chains studied by Nommenson et al. [54], PMMA particles grafted with poly(hydroxystearic acid) (PHS) studied by D'Haene [55] and the polystyrene–PNiPAM core–shell particles from our previous work [29], which had the same cross-link density in the shell as microgel M19. For the silica particles a hydrodynamic radius of 140 ± 5 nm with a

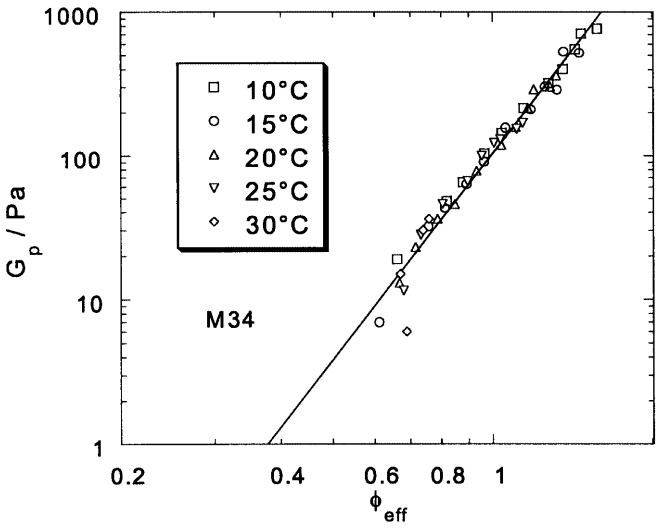

Fig. 11 Double-logarithmic plot of the plateau modulus against the effective volume fraction for microgel M34 with a power-law fit

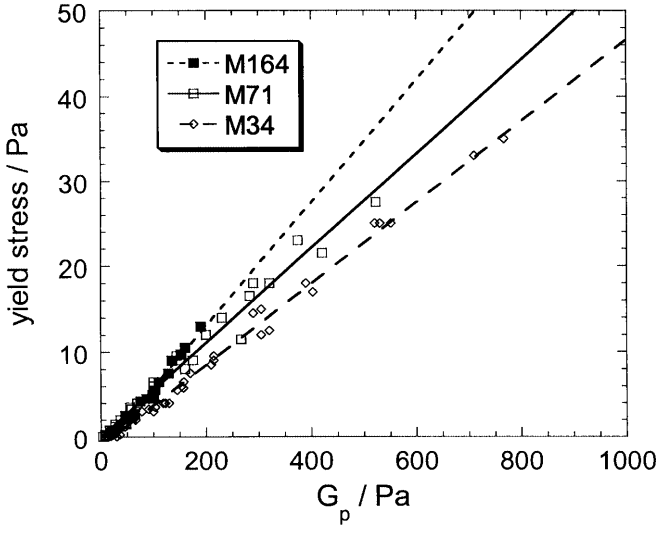

Fig. 12 Yield stress versus plateau modulus of the microgels

layer thickness of 58 nm and a polydispersity of about 4% was reported. D'Haene's PMMA particles were characterized by a particle radius of 65.5 nm and were coated with a PHS layer of 9-nm thickness with an overall polydispersity of 12%. The core–shell particle had a polystyrene core and a temperature-dependent, cross-linked PNiPAM shell with a size polydispersity of the core–shell particles of 12% at 25 °C as estimated from small-angle X-ray scattering measurements [56]. Whereas the other two systems have a maximum volume fraction of the zero-shear viscosity of 0.6, the core–shell system diverged at 0.65.

The viscoelastic properties can be characterized with the power-law behavior of the plateau modulus as a function of the volume fraction. Exponents of $m = 18$ for the PMMA particles, $m = 6$ for the grafted silica particles and $m = 5.7$ for the core–shell particles were found. The viscoelastic properties indicate that the PHS-grafted PMMA particles have a harder interaction potential than the silica particles and the polystyrene–PNiPAM core–shell particle. In contrast, the zero-shear viscosity of the first two systems diverged at the same volume fraction. When comparing the latter two systems (with about the same particle interaction potential as shown by a power-law coefficient of about $m = 6$) one can again deduce that the difference in ϕ_{max} (describing the divergence of η_0) is correlated with the size polydispersity, so the samples with a narrower particle size distribution have a lower ϕ_{max}.

The low-shear-rate and high-shear-rate viscosities of sterically stabilized systems were often used to characterize the softness of the stabilizing layer; however, our study on the temperature-sensitive microgels and the examples from the literature discussed previously indicate that the polydispersity of a colloidal system dominates the volume fraction of the limiting zero-shear viscosity, whereas the plateau modulus is more sensitive to the interaction potential of the systems considered. In order to be able to calculate the thickness of the stabilizing layer of a particle from the viscosity at high concentrations, one has to know the effective volume fraction, the interaction potential and the polydispersity of the particles because both a soft layer and a broad size distribution shift the divergence of shear viscosity (or in other words the maximum packing fraction) to higher values. Thus, the results presented here cast doubt on procedures that use the Krieger–Dougherty equation (Eq. 4) to determine the thickness of a steric layer.

Conclusions

In this contribution we reported the investigation of the influence of the cross-link density on rheological properties of temperature-sensitive microgels. Samples of PNiPAM microgels internally cross-linked with different amounts of BIS were prepared and characterized by SLS, DLS and DSC. The microgel suspensions were colloidally stable below the LCST of PNiPAM; however, the microgels flocculated when the LCST was reached. The temperature-dependent hydrodynamic radius revealed that the relative swelling decreased with increasing cross-link density.

Since the particle size strongly depends on the temperature, rheological properties, for example, viscosity, yield stress and storage modulus, decrease when the LCST is approached. The effective volume fraction of the microgel particles can be determined by fitting the relative viscosity of dilute solutions with the Einstein–

Batchelor equation. Then mastercurves are obtained for the viscosity and the plateau modulus for all cross-link densities over the whole temperature range, indicating that the particle interaction potential was not a function of temperature in the temperature range 10–30 °C.

The mastercurve of the zero-shear viscosity did not depend on the cross-link density and followed hard-sphere behavior up to an effective volume fraction of 0.5: apparently the nondraining limit was reached; however, the divergence of the zero-shear viscosity was found at higher effective volume fractions compared to hard spheres and is mainly determined by the polydispersity, which has a strong influence on the maximum volume fraction.

At high concentrations the microgel suspensions became viscoelastic. The plateau modulus also formed a temperature-independent mastercurve when plotted versus the effective volume fraction. However, the influence of the cross-link density and soft-sphere behavior was observed in contrast to the behavior of the zero-shear viscosity. The concentration dependence of the plateau modulus became weaker with decreasing cross-link density; thus, the particles became softer when they were less crosslinked.

Acknowledgements We thank the Bundesministerium für Bildung, Forschung und Technologie, the Deutsche Forschungsgemeinschaft and the Fonds der chemischen Industrie for financial support.

References

1. Antonietti M (1988) Angew Chem 100:1813
2. Funke WE, Okay O, Joos-Müller B (1998) Adv Polym Sci 138:139
3. Funke WE (1988) J Coat Technol 60/767:69
4. Bromley CWA (1989) J Coat Technol 61/768:39
5. Staudinger H, Husemann E (1935) Ber Dtsch Chem Ges 68:1618
6. Shashou VE, Beaman RG (1958) J Polym Sci 33:101
7. Wolfe MS, Scopazzi C (1989) J Colloid Interface Sci 133:265
8. Evans ID, Lips A (1990) J Chem Soc Farady Trans 86:3413
9. Rodriguez BE, Kaler EW, Wolfe MS (1992) Langmuir 8:2382
10. Bartsch E, Frenz V, Baschnagel J, Schärtel W, Sillescu H (1997) J Chem Phys 106:3743
11. Roovers J (1994) Macromolecules 27:5359
12. Buitenhuis J, Förster S (1997) J Chem Phys 107:262
13. Likos CN, Löwen H, Watzlawek M, Abbas B, Jucknischke O, Allgaier J, Richter D (1998) Phys Rev Lett 80:4450
14. Schild HG (1992) Prog Polym Sci 17:163
15. Tam KC, Ragaram S, Pelton RH (1994) Langmuir 10:418
16. Pelton RH, Hamielec AE, Woods DR, McPhee W, Wu X (1994) Colloid Polym Sci 272:467
17. Wu C (1998) Polymer 39:4609
18. Walter R, Ricka J, Quellet Ch, Nyffenegger R, Binkert Th (1996) Macromolecules 29:4019
19. Kiminta ÖDM, Luckham PF, Lenon S (1995) Polymer 36:4827
20. Kratz K, Eimer W (1998) Ber Bunsenges Phys Chem 102:848
21. Crowther HM, Saunders BR, Mears SJ, Cosgrove T, Vincent B, King SM, Yu G-E (1999) Colloids Surf A 152:327
22. Shibayama M, Tanaka T (1993) Adv Polym Sci 109:1
23. Jones MS (1999) Eur Polym J 35:795
24. Topp MDC, Hamse IM, Dijkstra PJ, Talsma H, Feijen J (1998) Polym Prepr Am Chem Soc Div Polym Chem 39:176
25. Chung JE, Yamato M, Yokoyama M, Aoyagi T, Sakurai Y, Okano T (1998) Polym Prepr Am Chem Soc Div Polym Chem 39:178
26. Ista LK, Perez-Luna VH, Lopez GP (1999) Appl Environ Microbiol 65:1603
27. Mielke M, Zimehl R (1998) Ber Bunsges Phys Chem 102:1698
28. Senff H, Richtering W, Norhausen Ch, Weiss A, Ballauff M (1999) Langmuir 15:102
29. Senff H, Richtering W (1999) J Chem Phys 111:1705
30. Inomata H, Wada N, Yagi Y, Goto S, Saito S (1995) Polymer 36:875
31. Nerger D, Burchard W, Schmidt M (1979) Polymer 20:582
32. Burchard W, Richtering W (1989) Prog Colloid Polym Sci 80:151
33. Kunz D, Burchard W (1986) Colloid Polym Sci 264:498
34. Lele AK, Hirve MM, Baginger MV, Mashelkar RA (1997) Macromolecules 30:157
35. Otake K, Inomata H, Konno M, Saito S (1990) Macromolecules 23:283
36. Murray M, Charlesworth D, Swires L, Cook J, Chowdhry BZ, Snowden MJ (1994) J Chem Soc Faraday Trans 90:1999
37. Batchelor GK (1977) J Fluid Mech 83:97
38. Cross M (1965) J Colloid Sci 20:417
39. de Kruif CG, van Iersel EMF, Vrij A, Russel WB (1985) J Chem Phys 83:4717
40. Rodriguez BE, Kaler EW, Wolfe MS (1992) Langmuir 8:2382
41. Krieger IM, Dougherty TJ (1959) Trans Soc Rheol 3:137
42. Quemada D (1977) Rheol Acta 16:82
43. Phan S-E, Russel WB, Cheng Z, Zhu J, Chaikin PM, Dunsmuir JH, Ottewill RH (1996) Phys Rev E 54:6633
44. Meeker SP, Poon WCK, Pusey PN (1997) Phys Rev E 55:5718
45. Duracher D, Elaissari A, Pichot C (1999) J Polym Sci Part A Polym Chem 37:1823
46. Bolhuis PG, Kofke DA (1996) J Phys Condens Matter 8:9627
47. Buscall R, Goodwin JW, Hawkins MW, Ottewill RH (1982) J Chem Soc Faraday Trans I 78:2873
48. Chen LB, CF Zukoski CF (1990) J Chem Soc Faraday Trans 86:2629
49. Zwanzig R, Mountain RD (1965) J Chem Phys 43:4464
50. Wagner NJ (1993) J Colloid Interface Sci 161:169
51. Bergenholtz J, Willenbacher N, Wagner NJ, Morrison B, van den Ende D, Mellema J (1998) J Colloid Interface Sci 202:430
52. Buscall R, Goodwin JW, Hawkins MW, Ottewill RH (1982) J Chem Soc Faraday Trans I 78:2889
53. Paulin SE, Ackerson BJ, Wolfe MS (1996) J Colloid Interface Sci 178:251
54. Nommenson PA, Duits MHG, Lopulissa JS, van den Ende D, Mellema J (1998) Prog Colloid Polym Sci 110:144
55. D'Haene P (1992) Dissertation. Universität Leuven, Belgium
56. Dingenouts N, Norhausen Ch, Ballauff M (1998) Macromolecules 31:8912